Hindawi

Research Article

A Numerical Analogy of Improving Efficiency for the PVT System in Bangladesh

F. T. Zohora [1,2] **and R. Nasrin** [1]

[1]*Department of Mathematics, Bangladesh University of Engineering and Technology, Dhaka 1000, Bangladesh*
[2]*Department of General Educational Development, Faculty of Science and Information Technology,*
 Daffodil International University, Daffodil Smart City, Ashulia, Dhaka, Bangladesh

Correspondence should be addressed to R. Nasrin; rehena@math.buet.ac.bd

Mathematical modeling of a three-dimensional PVT system is considered and solved using the FEM. Numerical simulation is applied to explore the influence of solar irradiance on the thermal energy, electrical power, and total efficiency of this system. Water is considered HTF. The solar irradiance, inlet fluid mass flow rate, ambient temperature, and partial shading are all chosen in the range of 200-500 W/m^2, 30-180 L/h, 10-37 °C, and 0-30%, accordingly based on the weather condition of Bangladesh. The effects of irradiance, fluid flow rate, ambient temperature, and partial shading on temperatures of cell and output fluid, electrical power and thermal energy, electrical efficiency-thermal efficiency, and total efficiency of this system are examined. Numerical results show that increasing each 100 W/m^2 solar irradiance enhances the cell and outlet temperatures and electrical and thermal energy by 2.17 and 0.54 °C and 20.7 and 113.3 W, respectively, and devalues the electrical, thermal, and overall efficiencies approximately 0.17, 0.67, and 0.83%, respectively. The cell and output water temperature reduce almost 0.6 and 0.83 °C, respectively; electrical and thermal energy rise by 0.30 and 3.07 W, respectively, and the electrical, thermal, and overall efficiencies escalate about 0.04, 0.4, and 0.44% for every 10 L/h mass flow rate increment. Due to each 10 °C increment of ambient temperature, cell and output water temperature increase 1.7 °C and 0.05 °C, electrical energy decreases to 0.9 W, thermal energy increases to 9.89 W, and electrical efficiency reduces about 0.1%.

1. Introduction

In the field of renewable energy, photovoltaic (PV) modules are among the most beneficial, long-lasting, and non-harmful technologies. It provides a longer service life while requiring the least amount of maintenance. PV components are inexpensive, simple to create, and enable production ranging from micro to megawatts. A 3D numerical system for a module of PV was developed and solved by Nasrin and Hossain [1] using COMSOL Multiphysics, a FEM technique-based software. According to their findings, for solar irradiance of 209 W/m^2, Rajshahi has the highest value of electrical power (15.14 W). At an irradiance intensity of 189 W/m^2, Sylhet has a maximum electricity efficiency of 12.85 percent. For every 1° increase in inclination angle, elec-

trical power and efficiency both fall by 0.06 W and 0.05%. The level of efficiency also declines from 14.66 to 11.32% as the area of partial shading increases from 0 to 40%. The electrical output and electrical efficiency of a PV module are affected by roughly 0.01 W and 0.01% for every 1 °C increase in solar cell temperature, respectively. Moreover, Rahman et al. [2, 3], El-Sebaii et al. [4], Hussein et al. [5], and Singh and Ravindra [6] also worked regarding this issue.

Nasrin et al. [7] demonstrate how a concentrator can improve the overall output of a PV module by enhancing the influence of high solar irradiance. Moreover, Nasrin et al. [8] also observed that, for raising irradiance from 1000 to 5000 W/m^2 with an optimal flow rate of 180 L/h, thermal and electrical energy rises from 1165 to 5387 W and 197 to 983 W, respectively. At the greatest irradiance level of

$5000 \, W/m^2$, thermal, electrical, and total efficiency are determined to be around 71, 10.6, and 81.6%, respectively.

Because of its endless supply, diversified conversion technologies, and environmentally beneficial nature, solar energy is widely regarded as the maximal promising alternative source of energy. A hybrid photovoltaic thermal (PV/T) system is a high-efficiency solar energy system that can produce both heat and electricity from a single physical structure. The hybrid collector's main challenge is to efficiently extract and transfer the heat. To overcome the above-mentioned difficulty, Nahar et al. [9] designed a PV/T system with a revolutionary design of a thermal collector that does not include the absorber plate. The outdoor experiment was done by them in Malaysia's typical climate, and a water elevation head has been employed to provide passive cooling for the photovoltaic module. The results of numerical simulations and experimental observations are found in better accordance. Under irradiance levels of $1000 \, W/m^2$ and the input and ambient temperatures of $34\,^\circ C$, the values of numerical and experimental analysis for the maximal total efficiency of the photovoltaic thermal system were determined to be 84.4% and 80%, respectively.

Additionally, only 15–20% of the irradiance impacting on the solar module is converted to electrical energy, with the rest being converted to heat and reducing electrical efficiency. Consequently, a hybrid PVT system is the best solution for harnessing both thermal and electrical energy. In addition, phase transition materials improve the cooling of PV cells and storage of heat. According to Fayaz et al. [10], the maximum electrical efficiency of a photovoltaic thermal system may be attained numerically and practically to be 12.4% and 12.28%, respectively. Similarly, the efficiency (η_e) of PVT-PCM is found to be 12.75% in the experimental case and 12.59% in this numerical scenario. The performance of electrical of the PVT system has improved by 10.13 and 9.2%, respectively. The electrical performance gain for PVT-PCM is calculated to be 12.91% mathematically and 12.75% empirically. According to Ashikuzzaman et al. [11], when PCM is employed in a photovoltaic thermal system, the temperature of the solar cell drops, as well as the output power and efficiency increase. Moreover, Fayaz et al. [12] also show that, when PCM is added to PVT system, the PV module reduces cell temperature by $12.6\,^\circ C$ to $10.3\,^\circ C$, numerically and experimentally, respectively. Maximum efficiency (η_e) achieved for PV is 13.72 and 13.56%, and for PVT, it is 13.85 and 13.74%, respectively. Furthermore, electrical efficiency is also reached empirically and numerically for PVT-PCM at 13.87 and 13.98%, respectively. Performance in electrical terms is enhanced by 6.2 and 4.8% in the PVT system and by 7.2 and 7.6% in the PVT-PCM system, numerically and empirically, respectively.

Photovoltaic thermal (PVT) systems face a few issues in maintaining the PV working temperature, one of which is effective cooling. Using nanofluids is one of the greatest strategies to raise the rate of heat transfer in the photovoltaic thermal system. Nasrin et al. [13] created a numerical model that may be used to construct several types of thermal collector systems using various materials. It has been determined that a PVT system based on nanofluid is more effective than a water-based one. Photovoltaic thermal systems using water/Cu, water/Ag, and water/Al nanofluids had a thermal efficiency of 7.08, 7.49, and 4.97%, respectively, as compared to water. Every $1\,^\circ C$ increment in input temperature reduces the recovered energy of thermal by 52.69, 53.13, 42.37, and 38.99 W for water/Al, water, water/Cu, and water/Ag nanofluids, respectively, from the PVT system. The heat flux from the heat exchanger to the cooling fluid increases by 27.45, 18.43, and 31.37% for the PVT. Furthermore, Nasrin et al. [14] also show that, by adopting a water-cooling system, the percentage of improved PV performance was found to be 9.2% in the experimental scenario. Using nanofluid instead of water results in higher thermal performance of about 4 and 3.67% in computational and experimental investigations, respectively. The total efficiency of the PV thermal system run by nanofluid at the irradiance level of $1000 \, W/m^2$ is found to be 89.2 and 87.65% during numerical and experimental research, respectively. Odeh and Behnia [15] also worked on this matter.

Partial shading has a variable impact on electricity generation of PV module and that impact on the performance of PV is investigated by Al Mamun et al. [16]. With a 25% shade and irradiance level of $600 \, W/m^2$, the impact factor of shading was 1.25, whereas, for 75% area of shading, it was 0.86. The electrical power production increased by 3.89, 3.37, 2.27, and 2.02 W at 0, 25, 50, and 75% shade, respectively, in terms of increasing irradiance $100 \, W/m^2$. At 75, 50, 25, and 0% shade, the level of efficiency raised by 0.22, 0.25, 0.27, and 0.29%. When the shaded area is increased by 10%, the power production drops by 12.41 W, and the electric efficiency drops by 2.3%. To improve the performance of PV, distributed maximum power point tracking (DMPPT) is a popular issue. Hanson et al. [17] used measured performance information for 542 photovoltaic systems to predict lost system performance owing to partial shade. The average power loss in order to shade for this analysis across 542 systems is 8.3%, and if the systems had not been outfitted with panel-level optimizers, the percentage would have risen to 13%. The usage of module-level dc power electronics has been projected to recover around 36% of the power wasted for shading. Moreover, Ahmed and Salam [18], Belhachat and Larbes [19], Bidram et al. [20], Dolara et al. [21], and Eke and Demircan [22] also worked regarding this issue. The use of cooling solutions to regulate the temperature level of PV modules is essential, and these should be cost-effective for the case of mega-installations. Shukla et al. [23] went into detail about various types of cooling techniques for photovoltaic panels, including hydraulic cooling, heat pipe cooling, natural and forced air cooling, thermoelectric cooling, and cooling with phase change materials. Moreover, Chandrasekar et al. [24] developed a method of passive cooling using cotton wick structures for stand-alone flat PV modules. Experimentally, the thermal and electric performance of a PV module with a cooling system made up of these wick structures in combination with CuO/water nanofluid, water, and Al_2O_3/water nanofluid is considered.

Furthermore, Hasanuzzaman et al. [25] compiled and reviewed the most recent literature on research projects that
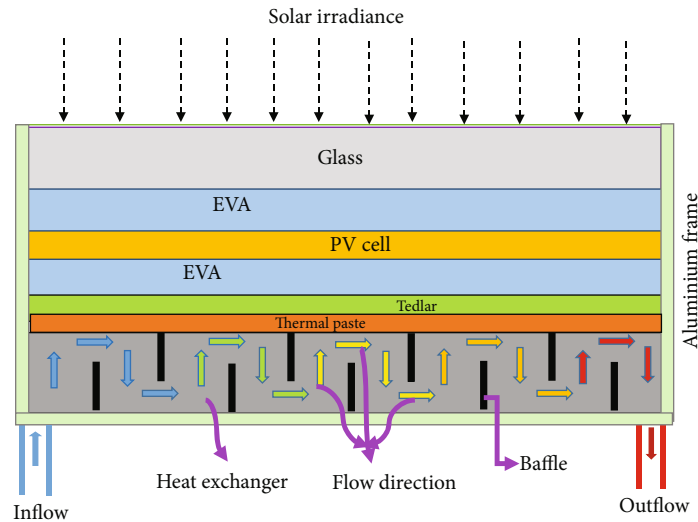
FIGURE 1: Two-dimensional view of the PVT system [8].

resulted in increased efficiency using appropriate cooling systems. Passive cooling solutions have been reported to reduce PV module temperature by 6–20 °C while rising electrical efficiency by up to 15.5%. However, cooling systems (active) perform better than cooling systems (passive), when the temperature of the PV module drops up to 30 °C, electrical efficiency is increased up to 22%, and thermal energy generation with an efficiency of up to 60%. In addition, Bahaidarah et al. [26] created a numerical model that was proven to be in accord with experimental climatic observations in Dhahran, Saudi Arabia. The module temperature was reduced by nearly 20% with active water cooling, resulting in a 9% gain in PV panel efficiency.

Many scholars have conducted numerous numerical, analytical, and experimental studies to examine the various operating parametric effects to investigate the probable strategies for improving PV module performance. Only 15-20% of the irradiance intensity of the panel is changed into electricity in experiments, and the rest is turned into heat (Jie et al. [27]; Teo et al. [28]). Irradiance intensities were randomly set to establish partial shade conditions via simulation on an array consisting of a panel, according to Parlak [29]. The proposed algorithm for the highest irradiance intensities and array configurations resulted in a 37.1% improvement in power production. Ishaque et al. [30] compared the accuracy of partial shading modeling to the accuracy of three distinct types of modeling methodologies. In addition, a PV array with controllers and power converters is modeled. The results of experimental research were found to have a close agreement with the theoretic prediction. The algorithm is simplified using the graphical technique.

A two-axis (open-loop) movable PV solar tracker is constructed and evaluated by Kivrak et al. [31]. For the tilted angle 37 °C in Denizli, Turkey, the performance of the PV module is theoretically and empirically tested, and for the moving purpose of the solar tracker, two DC actuator motors have been used. They showed that the production of energy for a two-axis moving PV panel increased by about 64% when compared to the fixed photovoltaic system. Fur-

thermore, Gómez-Gil et al. [32], Rustemli et al. [33], Mousazadeh et al. [34], and Mamlook et al. [35] also worked regarding this topic. The impact of forced convection on the thermal and electric efficiency of a single-pass air PVT system was examined experimentally by Kasaeian et al. [36]. A PVT system with a customized air-cooling with four fans to provide forced convection conditions was tested for this purpose. Their results showed that decreasing the thickness of the air channel improves the efficiency of thermal but has no significant impact on the efficiency of electrical. The thermal efficiency of a system with an air mass flow rate ranging from 0.018 (kg/s) to 0.06 (kg/s) and a 0.05 (m) channel depth is roughly 15–31%, while the electrical efficiency is only 12–12.4%. All the researchers of Hosenuzzaman et al. [37], Jahn and Nasse [38], Kelly and Gibson [39], MacAlpine et al. [40], and Rasachak et al. [41] conducted studies based on performance/efficiency enhancement of PV/PVT system under different environmental/operational uniform/non-uniform conditions by indoor/outdoor experiments in Malaysia, global aspect, Germany, etc.

Numerical/experimental research based on PV/PVT systems in Bangladesh is still at the nursery level. More investigations are necessary. The objective of this study is to investigate the performance of the solar PVT system numerically within various operational circumstances in Bangladesh. The novelty of this research is to find the solution of the 3D mathematical model numerically for the PVT system and also discover the overall performance of the PVT system in the operating condition of Bangladesh.

2. Framework of Mathematical Model

The considered PVT system in two-dimensional view is expressed in Figure 1 where the two-dimensional sketch of the PV module and the heat exchanger are shown along the zx and the yx direction, respectively. The geometrical and physical properties of the PV module (E310P(S)-011 of EPV brand, Malaysia) are used for the present numerical research. The module has 72 (6∗12) solar polycrystalline

TABLE 1: The measurements and material criteria of the PVT [3, 8, 9].

Materials	Measurement (m)	Density	Specific heat	Thermal conductivity
Glass	$1.9 \times 1 \times 0.003$	2450	500	2
EVA	$1.9 \times 1 \times 0.0008$	950	2090	0.311
Polycrystalline cell	$1.9 \times 1 \times 0.0001$	2329	700	148
Tedlar	$1.9 \times 1 \times 0.00005$	1200	1250	0.15
Thermal paste	$1.7 \times 1 \times 0.0003$	2600	700	1.9
Heat exchanger	$1.7 \times 1 \times 0.012$	237	900	2700
Inlet-outlet pipes	$0.05 \times 0.01 \times 0.01$	237	900	2700
Baffles	$0.978 \times 0.001 \times 0.01$	237	900	2700
Fluid region	$1.698 \times 0.998 \times 0.01$	998	4200	0.68

TABLE 2: PVT properties [3, 8, 16].

Criteria	Value
τ_g	0.96
ε_g	0.04
α_{sc}	0.9
α_{td}	0.5
η_{sc} (%)	0.13
μ_{SC}	0.0045
T_{amb} (°C)	27
T_{in} (°C)	27
T_r (°C)	25
P_{sc}	20%
Area of each cell (m²)	0.156*0.156
PVT area, A (m²)	8.76
Number of cells	6*12
PV layers thermal transfer coefficient, U_t (W/m²K)	150
U_{td} (W/m²K)	77
U_{hea} (W/m²K)	5.84
U_{he} (W/m²K)	66

1*10 mm). The measurements and material properties of the PVT are enlisted in Tables 1 and 2.

The governing equations of the PVT system [8] are as follows:

$$
-\left(\frac{k}{\rho c_P}\right)_g \left(\frac{\partial^2 T_g}{\partial x^2} + \frac{\partial^2 T_g}{\partial y^2} + \frac{\partial^2 T_g}{\partial z^2}\right)
$$
$$
= \alpha_g G - U_{g\alpha}\left(T_g - T_{amb}\right) - \varepsilon_g \sigma \left(T_g^4 - T_s^4\right) - U_t\left(T_g - T_{sc}\right),
\tag{1}
$$

$$
-\left(\frac{k}{\rho c_P}\right)_{sc} \left(\frac{\partial^2 T_{sc}}{\partial x^2} + \frac{\partial^2 T_{sc}}{\partial y^2} + \frac{\partial^2 T_{sc}}{\partial z^2}\right)
$$
$$
= \alpha_{sc} \tau_g G - E_e - U_t\left(T_{sc} - T_{td}\right) - U_t\left(T_{sc} - T_g\right),
\tag{2}
$$

$$
-\left(\frac{k}{\rho c_P}\right)_{td} \left(\frac{\partial^2 T_{td}}{\partial x^2} + \frac{\partial^2 T_{td}}{\partial y^2} + \frac{\partial^2 T_{td}}{\partial z^2}\right)
$$
$$
= U_t\left(T_{sc} - T_{td}\right) - U_{td}\left(T_{td} - T_{he}\right),
\tag{3}
$$

$$
-\left(\frac{k}{\rho c_P}\right)_{he} \left(\frac{\partial^2 T_{he}}{\partial x^2} + \frac{\partial^2 T_{he}}{\partial y^2} + \frac{\partial^2 T_{he}}{\partial z^2}\right)
$$
$$
= U_{td}\left(T_{td} - T_{he}\right) - U_{he}\left(T_{he} - T_f\right) - U_{hea}\left(T_{he} - T_{amb}\right),
\tag{4}
$$

$$
\frac{\partial u}{\partial x} + \frac{\partial v}{\partial y} + \frac{\partial w}{\partial z} = 0,
\tag{5}
$$

$$
u\frac{\partial u}{\partial x} + v\frac{\partial u}{\partial y} + w\frac{\partial u}{\partial z} = -\frac{1}{\rho}\frac{\partial p}{\partial x} + \nu\left(\frac{\partial^2 u}{\partial x^2} + \frac{\partial^2 u}{\partial y^2} + \frac{\partial^2 u}{\partial z^2}\right),
\tag{6}
$$

$$
u\frac{\partial v}{\partial x} + v\frac{\partial v}{\partial y} + w\frac{\partial v}{\partial z} = -\frac{1}{\rho}\frac{\partial p}{\partial y} + \nu\left(\frac{\partial^2 v}{\partial x^2} + \frac{\partial^2 v}{\partial y^2} + \frac{\partial^2 v}{\partial z^2}\right),
\tag{7}
$$

cells, size of each cell (156*156 mm), maximum power 295 W, weight 22 Kg, dimension (1984*997*42 mm), extreme power voltage 30.6 V, extreme power current 8.17 A, open-circuit voltage 45.7 V, and short circuit current 8.92 A. The PV layers are glass top cover, ethylene-vinyl acetate (EVA)-1 layer, polycrystalline silicon layer, EVA-2 layer, and tedlar polyvinyl fluoride (PVF) layer. The thickness of PV surfaces is of glass (3 mm), polycrystalline cell (0.1 mm), EVA (0.8 mm), and tedlar (0.05 mm). A heat exchanger (box-shaped of 1-mm thickness at every side) is attached to the PV bottommost layer applying thermal paste. Sixteen baffles are inserted inside the heat exchanger with each gap of 100 mm. Heat exchangers, inlet-outlet headers, and baffles are made of aluminum. The inlet and outlet header pipes are of rectangular shaped. The dimension is of heat exchanger (1700*1000*12 mm), of input-output header pipes (50*10*10 mm), and of baffles (978*
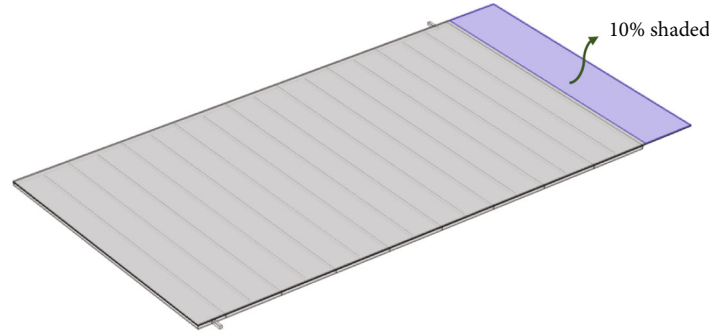
FIGURE 2: Three-dimensional computational view of the PVT system with 10% shaded area.

$$u \frac{\partial w}{\partial x} + v \frac{\partial w}{\partial y} + w \frac{\partial w}{\partial z}$$
$$= -\frac{1}{\rho} \frac{\partial p}{\partial z} + v \left(\frac{\partial^2 w}{\partial x^2} + \frac{\partial^2 w}{\partial y^2} + \frac{\partial^2 w}{\partial z^2} \right), \quad (8)$$

$$(\rho C_p) \left(u \frac{\partial T_f}{\partial x} + v \frac{\partial T_f}{\partial y} + w \frac{\partial T_f}{\partial z} \right)$$
$$= k \left(\frac{\partial^2 T_f}{\partial x^2} + \frac{\partial^2 T_f}{\partial y^2} + \frac{\partial^2 T_f}{\partial z^2} \right), \quad (9)$$

where $\sigma = 5.670367 \times 10^{-8} \text{W/m}^2\text{k}^4$ and $T_s = 0.0552 T_{amb}^{1.5}$ are the Stefan-Boltzmann constant and the sky temperature, respectively.

The governing equations (1-4) represent how the solar irradiance is received by the PVT surface and distributed among the PVT layers specially for the glass, solar cell, tedlar, and heat-exchanger layers, respectively. The next equations (5-8) represent the laminar, viscous and incompressible flow pattern for the fluid domain only. Then, Equation (9) displays the heat transfer for the fluid. Thus, using the energy balance equations (1-4, 9) and the fluid flow equations (5-8), the mechanism is described of how the electrical power and thermal energy are converted and collected from the source of the solar irradiance by the considered PVT system from layer to layer.

$$\text{Total received energy by the PVT system} : E_r = \tau_g \alpha_{sc} p_{sc} GA, \quad (10)$$

$$\text{Solar cell temperature} : T_{sc}$$
$$= \frac{p_{sc} G (\tau_g \alpha_{sc} - \eta_{sc}) + (U_{ga} T_a + U_{gtd} T_{td})}{(U_{ga} + U_{gtd})}, \quad (11)$$

$$\text{Electrical power} : E_P = \eta_{SC} \rho_{SC} \tau_g \alpha_{SC} GA [1 - \mu_{SC}(T_{SC} - T_r)], \quad (12)$$

$$\text{Thermal energy} : E_t = m c_p [T_{out} - T_{in}], \quad (13)$$

$$\text{Electrical efficiency} : \eta_e = \frac{\text{Produced electrical power}}{\text{Total received energy}} = \frac{E_P}{E_r}, \quad (14)$$
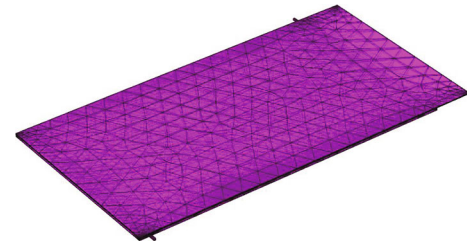

FIGURE 3: Finite element meshing of a PVT system.

TABLE 3: Grid sensitivity check at $G = 500 \text{ W/m}^2$ and $V_{in} = 180$ L/h.

No. of elements	38,882	87,585	154,210	**253,276**	421,903
T_{sc} (°C)	38.053	38.424	38.872	39.011	39.012
T_{out} (°C)	29.143	29.325	29.561	29.735	29.7351
Time (s)	98	177	254	323	405

$$\text{Thermal efficiency} : \eta_t = \frac{\text{Generated thermal energy}}{\text{Total received energy}} = \frac{E_t}{E_r}, \quad (15)$$

$$\text{Overall efficiency} : \eta_o = \eta_e + \eta_t = \frac{E_p + E_t}{E_r}. \quad (16)$$

Boundary conditions according to [8]:

$$\text{PVT side boundaries} : -n \cdot (k\Delta T) = 0,$$
$$\text{PVT glass surface} : \text{inward heat flux} - k_g \frac{\partial T_g}{\partial z} = G,$$
$$\text{Fluid domain's solid surfaces} : u = v = w = 0,$$
$$\text{Fluid} - \text{solid border} : k_f \left(\frac{\partial T}{\partial d} \right)_f = k_{he} \left(\frac{\partial T}{\partial d} \right)_{he}, \quad (17)$$
$$\text{Inlet} : T = T_{in}, u = 0, v = V_{in}, w = 0,$$
$$\text{Outlet} : p = 0,$$

where d is the surface normal distance and acts along with coordinate axes' directions.

Figure 2 represents the three-dimensional computational view of the PVT system where 10% area of PV is shaded. Similarly for 20% and 30% partial shading cases, the shaded
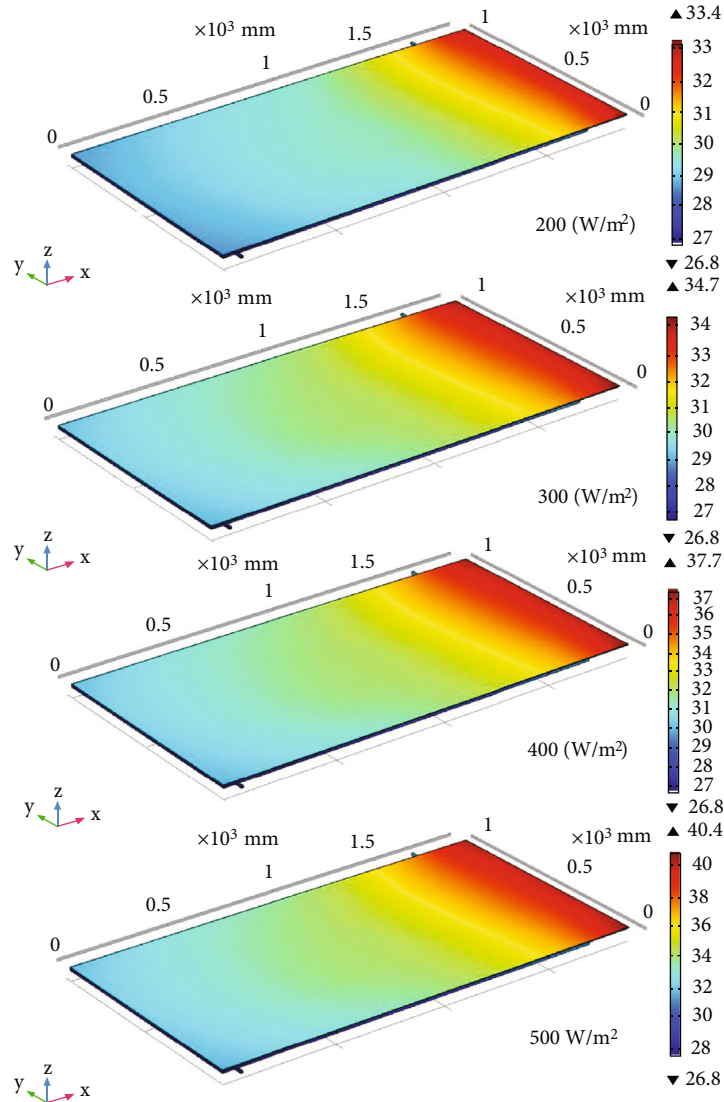
FIGURE 4: Outcome of irradiance on PVT surface temperature with $V_{in} = 180$ L/h, $T_{amb} = 27°C$, and no partial shading.

area enhances from right to left side of the PV module. For the numerical simulation the shaded area is chosen as a continuous domain though practically the shaded area may be a scattered domain.

3. Computational Procedure

Galerkin's weighted residual FEM [42] is used for solving governing nonlinear PDEs (1)-(9). Solving the mass conservation, energy conservation, and momentum equations, we can find out the temperature of the solar cell (T_{sc}), output fluid (T_{out}), the pressure (p), and velocity (u, v, w) of fluid in the PVT system. The convergence criterion is set as $|\psi^{n+1} - \psi^n| \leq 1.0e^{-4}$.

3.1. Generation of the Mesh.
Figure 3 depicts the finite element meshing of a PVT module's computational domain. The subdomain and boundary elements in this numerical model are free tetrahedral and free triangular forms, respec-

tively. Ten and six nodes are used for tetrahedral and triangular elements, respectively. From the mesh statistics, we find that the computational geometry consists of 186980 tetrahedral, 68649 triangles, 858 pyramids, 65438 prisms, 168 quads, 6978 edge elements, and 202 vertex elements. Thus, the total no of elements is 253276. The average element quality is 0.3829, the element mass ratio is 1.231E-8, and the mesh mass is 2.994E7 mm^3.

3.2. Independence Test of the Grid.
The grid of the PVT system is tested using $G = 500 W/m^2$ and $V_{in} = 180 L/h$. Elements 38,882, 87,585, 154,210, 253,276, and 421,903 are used to check several forms of non-uniform grid systems. Cell temperature and outflow fluid temperature are used as monitoring parameters. The findings of cell and water output temperatures are not differed significantly between last two columns, but the simulated time is unacceptable. Table 3 shows the outcome of the grid test. Thus, the grid system of 253,276 elements is used.
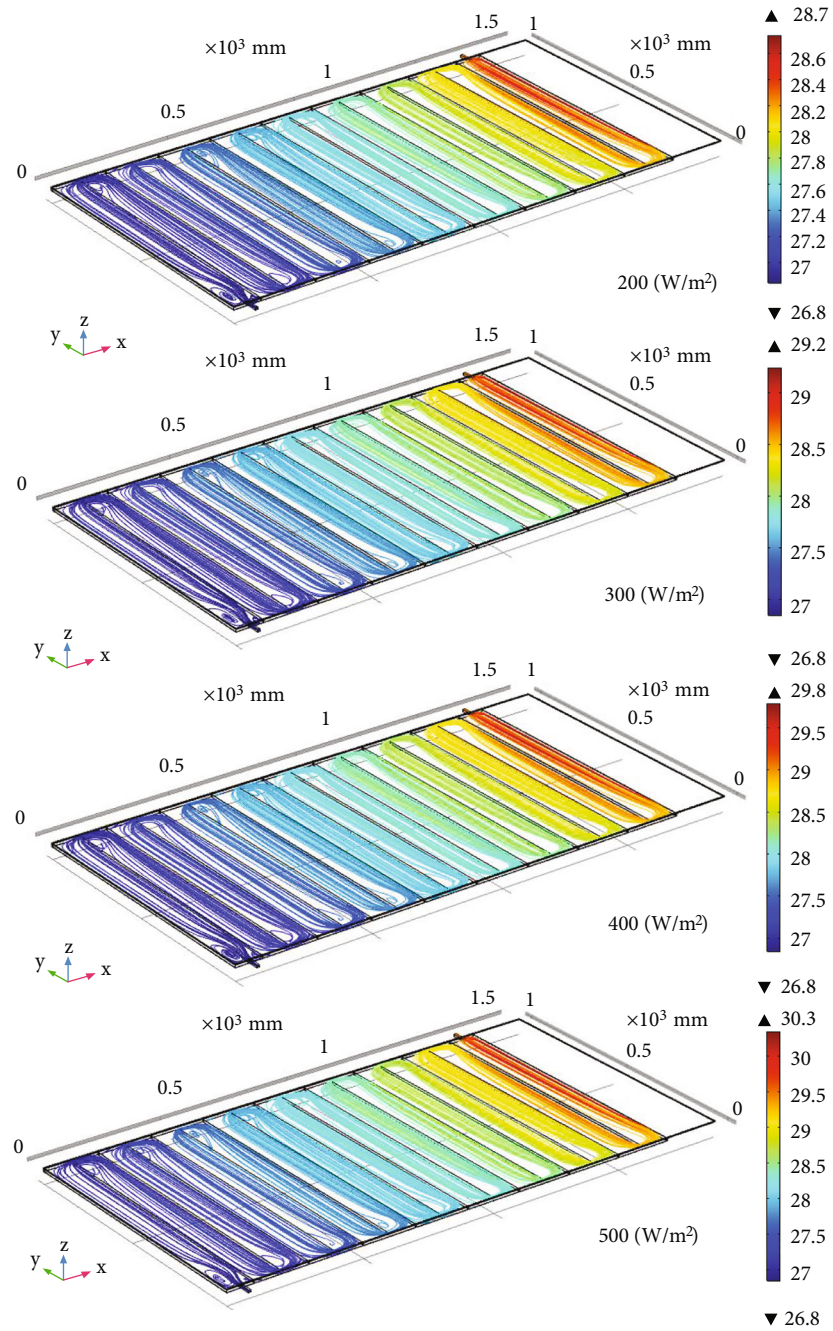
Figure 5: Outcome of irradiance on PVT streamlines plot with $V_{in} = 180$ L/h, $T_{amb} = 27°$C, and no partial shading.

3.3. *Verification of Code.* The code validation is shown in Nasrin et al. [8], which is not repeated in this article.

4. Outcomes

Bangladesh is a state of huge sunlight; however, the accessibility to a power resource is not great, if the essential technology to tie energy together is not accessible. The graphical location of this country is latitude between 20°34' and 26°38' North and longitude between 88°01' and 92°41' East. Its climate is tropical. Bangladesh is a fine receiver of solar energy due to its location. Its total area is 1.49E+11 m² and receives monthly average irradiance of 5 KWh/m² by this land per year. Throughout the last decades, significant advances in various solar energy machinery have been done, and already some have attained the commercial phase. Monthly irradiance (KWh/m²) at different positions of Bangladesh has been shown in Nasrin and Hossain [1, 43]. The highest amount of solar irradiance all over Bangladesh has been monitored in May and the smallest amount in December. Thus, yearly average irradiance for Dhaka, Rajshahi, Sylhet, Chittagong, Barisal, and Khulna have been calculated and found as 197, 209, 189, 192, 196, and 202 W/m²,
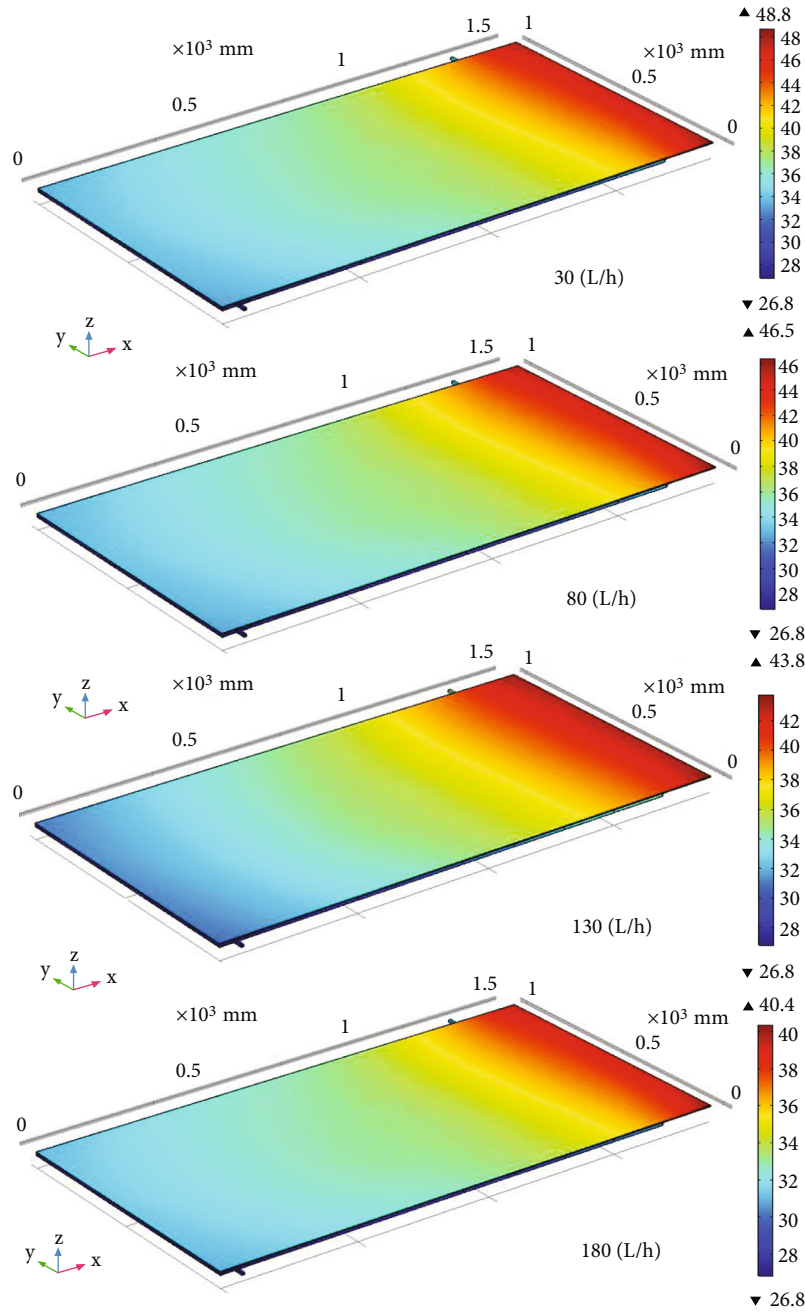
FIGURE 6: Outcome of mass flow rate on PVT surface temperature with $G = 500$ W/m^2, $T_{amb} = 27°$C, and no partial shading.

respectively. Solar irradiance, inlet fluid mass flow rate, input fluid temperature, and partial shading are all examined in the range of 200-500 W/m^2, 30-180 L/h, 10-37°C, and 0-30%, accordingly.

4.1. Outcome of Irradiance.
The consequence of solar irradiance (G) on the temperature in terms of the surface temperature plot is depicted in Figure 4. The considered standards of G are from 200 W/m^2 to 500 W/m^2 at the stable flow rate of inlet fluid 180 L/h, ambient temperature 27°C, and partial shading 0%. The range of surface temperature is found from 26.8 to 33.4°C for 200 W/m^2 of G, from 26.8 to 34.7°C for

300 W/m^2 of G, 26.8 to 37.7°C for 400 W/m^2 of G, and from 26.8 to 40.4°C for 500 W/m^2 of G, respectively.

Figure 5 shows the streamlines plot of the PVT system with a cooling system for several values of G from 200 W/m^2 to 500 W/m^2 at a fixed rate of inlet fluid 180 L/h. When G is 200 W/m^2, the range of fluid temperature is found from 26.8 to 28.7°C, from 26.8 to 29.2°C when G is 300 W/m^2, from 26.8 to 29.8°C when G is 400 W/m^2, and from 26.8 to 30.3°C when G is 500 W/m^2, respectively. There is also a color expression for the streamlined plot. The temperature bar (°C) can be used to calculate the temperature of the fluid. With increasing irradiance values, the
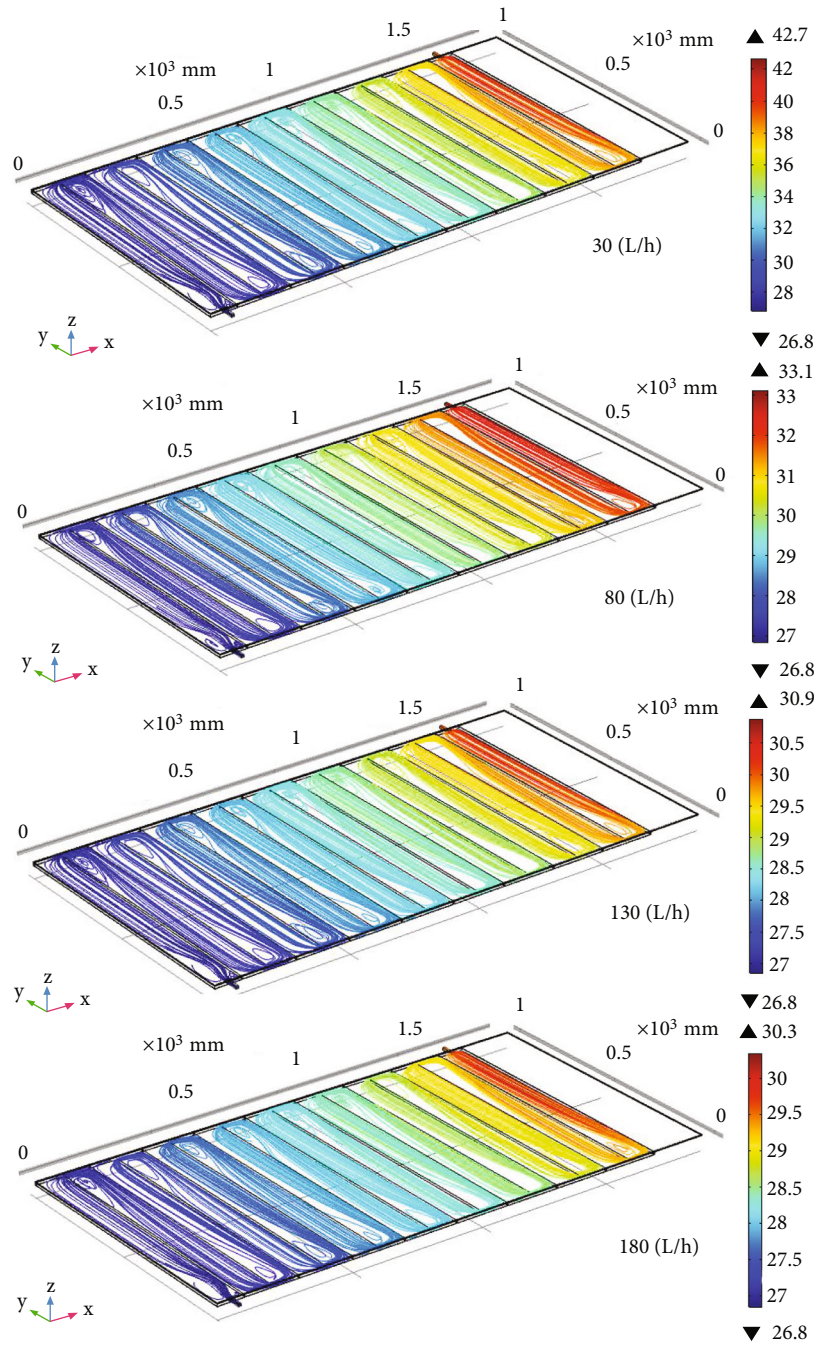
FIGURE 7: Outcome of mass flow rate on PVT streamlines plot with $G = 500 \text{ W/m}^2$, $T_{amb} = 27°C$, and no partial shading.

average T_{out} rises because the increased solar irradiance raises the T_{sc} of PV.

4.2. Outcome of Mass Flow Rate.
Figure 6 displays the effect of the mass flow (inlet) rate on the surface temperature plot for the PVT system at 500 W/m^2 of G, $27°C$ of T_{amb}, and 0% of partial shading. The mass flow rates considered as 30, 80, 130, and 180 L/h which correspond to 0.00085, 0.023, 0.037, and 0.051 m/s, respectively. The range of PVT surface temperature is found from 26.8 to 48.8 °C for the flow rate 30 L/h, from 26.8 to 46.5 °C for

flow rate 80 L/h, 26.8 to 43.8 °C for the flow rate 130 L/h, and from 26.8 to 40.4 °C for flow rate 180 L/h, respectively. From the figure, it is discovered that when the mass flow rate (inlet) increases, the highest temperature of the PVT material slowly declines. Growing temperature is maximum at the least flow rate (30 L/h) and minimum at the highest flow rate (180 L/h). This is the case for fluid flow parameters that have a dominant behavior. Thus, conductive and convective heat transfer processes proceed through the heat exchanger of PVT from the glass surface to the outlet.
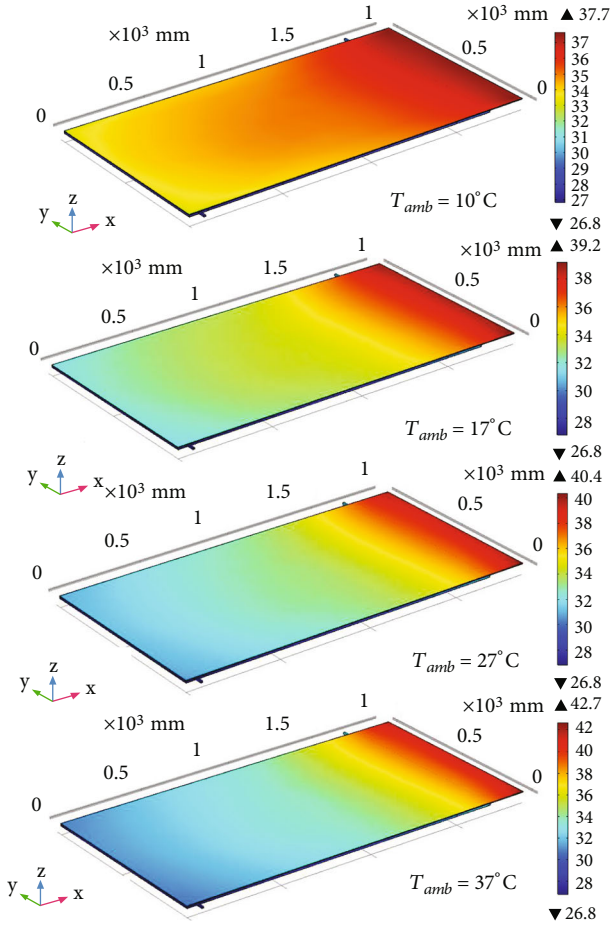
FIGURE 8: Outcome of ambient temperature on PVT surface temperature with $G = 500 \, \text{W/m}^2$, $V_{\text{in}} = 180 \, \text{L/h}$, and no partial shading.

Figure 7 shows the streamlines plot of the system with the cooling system at various mass flow rates where G is set to $500 \, \text{W/m}^2$. The T_f at the outlet increases when the rate of mass flow is reduced. As the mass flow rate increases, the temperature of the fluid decreases. This is significant because a rapidly flowing fluid is incapable of absorbing the additional heat from the heat exchanger of the system. The fluid flow distribution from the inlet port to the outlet port is depicted in this diagram. The range of fluid temperature is found from 26.8 to 42.7 °C for the flow rate 30 L/h, from 26.8 to 33.1 °C for flow rate 80 L/h, 26.8 to 30.9 °C for the flow rate 130 L/h, and from 26.8 to 30.3 °C for flow rate 180 L/h, respectively.

4.3. Outcome of Ambient Temperature. Figure 8 depicts the outcome of T_{amb} on a PVT system in terms of surface temperature plot. The ambient temperature (T_{amb}) is measured at 10, 17, 27, and 37 °C. This temperature range covers the whole six-season temperature range of Bangladesh. In this scenario, the sun irradiance is set at $500 \, \text{W/m}^2$, the flow rate is set to 180 L/h, and partial shading is 0%. The temperature of the surface of the system rises from 26.8 to 37.7 °C at 10 °C ambient temperature. Similarly, it rises from 26.8 to 39.2 °C

at 17 °C ambient temperature, from 26.8 to 40.4 °C at 27 °C ambient temperature, and from 26.8 to 42.7 °C at 37 °C ambient temperature.

The impact of T_{amb} on the PVT system is shown in Figure 9 in terms of the streamlines plot. The fluid temperature of the system rises from 26.8 to 29.8 °C at 10 °C ambient temperature. Similarly, it rises from 26.8 to 30 °C at 17 °C ambient temperature, from 26.8 to 30.3 °C at 27 °C ambient temperature, and from 26.8 to 30.6 °C at 37 °C ambient temperature. Thus, whenever ambient temperature increases, convective heat transfer from the PVT boundaries to the ambient becomes lesser as a result the PVT surface temperature increases, and we get higher hot output water.

4.4. Outcome of Partial Shading. Figure 10 shows the effect of partial shading from 0% to 30% on the PVT system at a constant level of G of $500 \, \text{W/m}^2$, the mass flow rate of 180 L/h, and T_{amb} of 27 °C in terms of surface temperature plot. The figure shows that the solar shade area has a substantial impact which is disproportional on the surface temperature of the PVT system. For 0, 10, 20, and 30% partial shading, the range of surface temperature of PVT modules is 26.8 to 40.4 °C, 26.8 to 39.6 °C, 26.8 to 39.2 °C, and 26.8 to 38.7 °C, respectively.

The result of partial shading on the PVT system is shown in Figure 11 in terms of streamlines plot at a fixed G of $500 \, \text{W/m}^2$. In 0% shading, the temperature of heat transferring fluid rises from 26.8 to 30.3 °C. On the other hand, after reaching 10% shading, T_f declines from 26.8 to 30 °C. When the PVT area is shaded 20%, the T_f drops from 26.8 to 29.9 °C. Finally, the temperature of water dropped from 26.8 to 29.8 °C in the case of a 30% shading area of PVT top surface.

4.5. Cell Temperature. The T_{sc} is presented in Figures 12(a)–12(d) for the effect of G, flow rate, T_{amb}, and partial shading, respectively. It is obvious from Equation (11) that the average T_{sc}, the surface temperature of the heat exchanger, T_{amb}, and incident irradiance all have a strong relationship.

Figure 12(a) shows that, for the variation of irradiance from 200 to $500 \, \text{W/m}^2$, T_{sc} rises by 6.5 °C in the PVT system with a cooling system of 180 L/h flow rate and T_{in} of 27 °C. The current results indicate that each $100 \, \text{W/m}^2$ growth in G raises the T_{sc} by around 2.17 °C. The objective of this study is to keep T_{sc} within a particular sort by employing a suitable cooling system so that the PV material does not degrade.

Figure 12(b) depicts that, at the irradiance level 500 W/ m^2, input fluid temperature 27 °C, the cell average temperature water decreases as the inlet fluid mass flow rate increases from 30 to 180 L/h. Convection removes more heat from the system when the incoming fluid flow rate is raised. Consequently, the average T_{sc} has been reduced. The cell means temperature drops fast as the flow rate increases, as shown in this graph. The flow rate is initially 30 L/h, and T_{sc} is 48 °C. Additionally, the T_{sc} regularly drops up to a flow rate of 180 L/h. The temperature T_{sc} drops by 0.6 °C for every 10 L/h growth in incoming fluid mass flow rate.

Figure 12(c) shows that convective heat transfers from the system to the ambient air decreases as the T_{amb} (10-
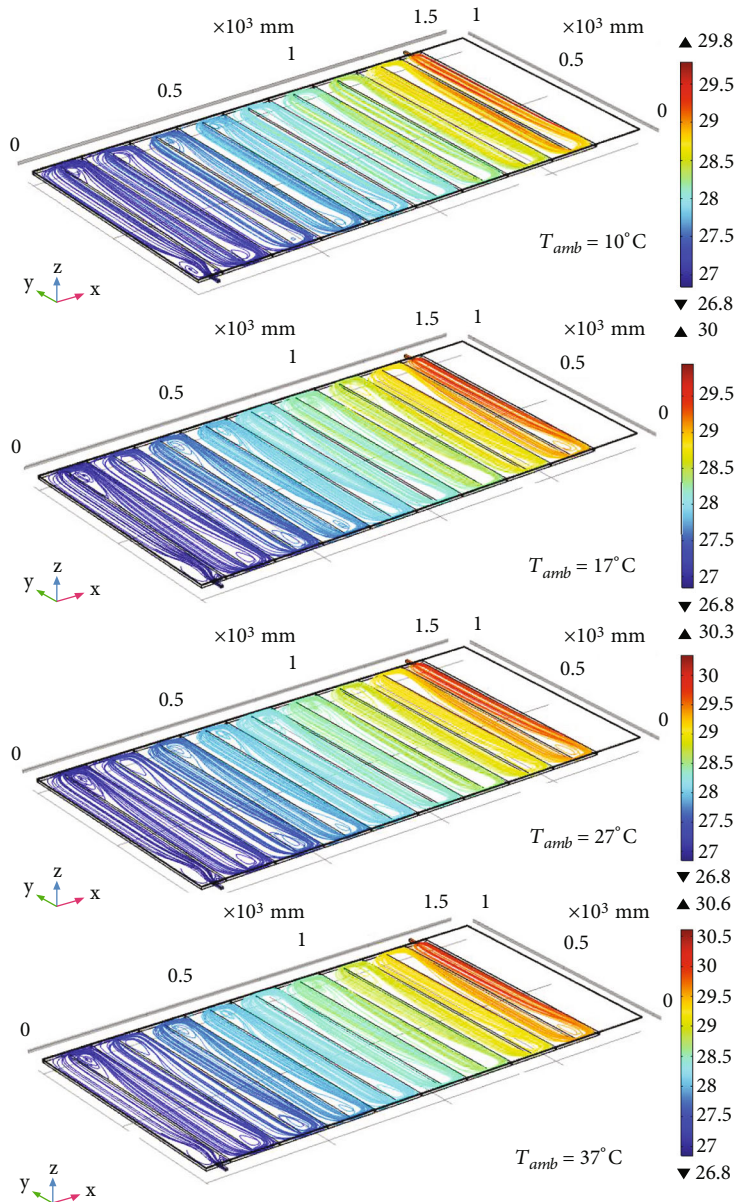
FIGURE 9: Outcome of ambient temperature on PVT streamlines plot with $G = 500$ W/m^2, $V_{in} = 180$ L/h, and no partial shading.

37 °C) rises. As a result, convection removes less heat from the system which enhances the average T_{sc} to around 36.5, 38, 39, and 41 °C for ambient temperatures of 10, 17, 27, and 37 °C, respectively. For every 10 °C increase in T_{amb}, T_{sc} increased about 1.67 °C.

The solar cell temperature (T_{sc}) of the PVT system is 39 °C when there is no shade, as shown in Figure 12(d). When partial shading is increased from 10 to 30%, the cell temperature drops to 38.6 °C, 38.2 °C, and 37.8 °C. Therefore, T_{sc} decreases by 0.4 °C for every 10% shading condition of the PVT system.

4.6. Electrical Power. Figures 13(a)–13(d) show the total amount of E_p (W) produced for various irradiance G (200-500 W/m^2), mass flow rate (30-180 L/h), T_{amb} (10-40°C), and partial shading (0-30%). Figure 12(a) shows that the

starting level of G is 200 W/m^2 and the output power is 43.58 W, while the E_p is 105.65 W at the level of 500 W/m^2. The electrical power of a PVT system with a cooling system at a flow rate of 180 L/h and T_{in} of 27 °C increases by 20.69 W for every 100 W/m^2 rises in the level of G. This happens due to the PV module's size, P, T_{ref}, operating conditions, improper cooling system installation, and material qualities.

Figure 13(b) depicts that the primary flow rate is 30 L/h and the E_p is 101.08 W at a fixed G level of 500 W/m^2 in various fluid mass flow rates. The output power rises to 105.65 W at a peak flow rate of 180 L/h. With an increase in fluid mass flow rate of about 150 L/h, the output power increases by 4.57 W. For every 10 L/h increase in fluid flow rate, the output power rose by 0.30 W under cooling conditions.
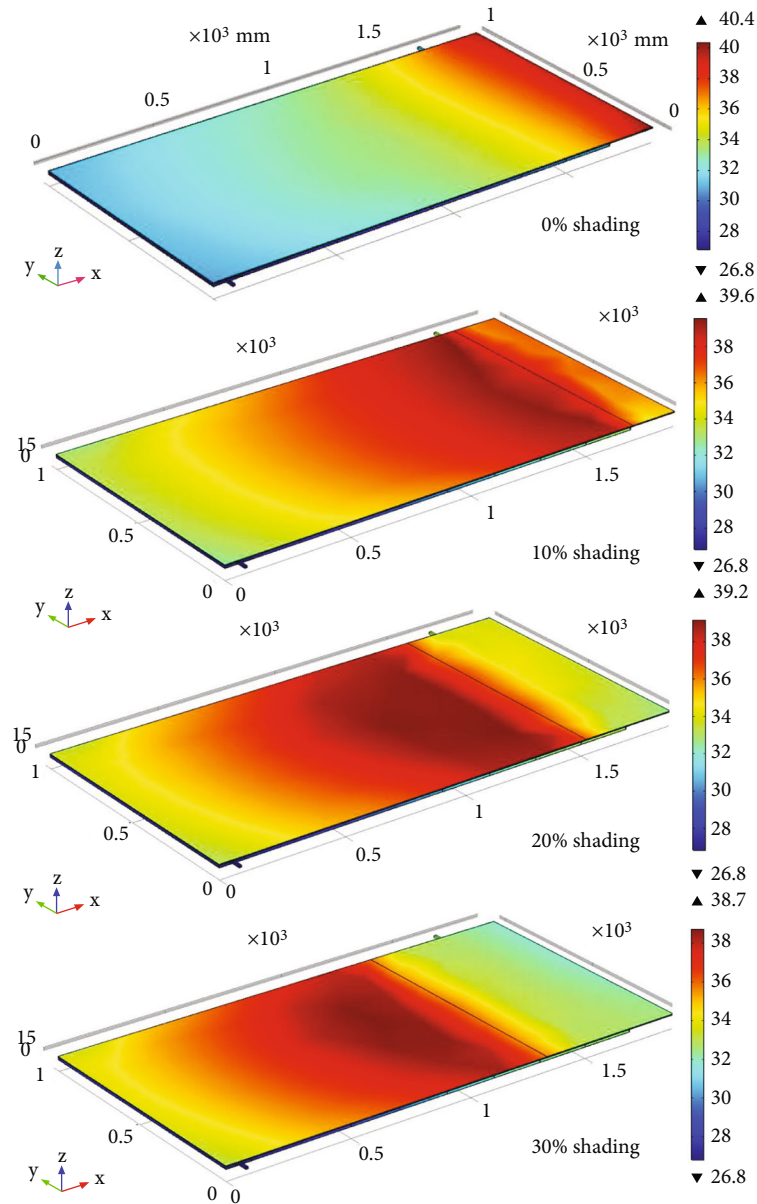
FIGURE 10: Outcome of partial shading on PVT surface temperature with $G = 500$ W/m^2, $V_{in} = 180$ L/h, and $T_{amb} = 27$°C.

Figure 13(c) shows the change of electrical power (E_p) as a function of T_{amb}. For rising T_{amb} values from 10 to 37 °C, the electrical power (E_p) against above ambient temperature is 107, 106, 105.65, and 104.6 W, respectively. For each 10 °C increase in ambient temperature, electrical power decreased by about 0.9 W. As the ambient temperature rises, the convective heat transfer phenomenon decreases. Thus, the electrical power generation of the PVT system is showing a downward trend.

Figure 13(d) shows that the electrical power output is 105.65 W at a 500 W/m^2 level of G and has no shading conditions. The electrical power output was reduced to 95.27 W after attaining 10% shade. When 20% of the PVT area is shaded, the electrical power drops to 84.84 W. Finally, when 30% of the PVT top surface is shaded, the electrical power

production drops to 74.38 W. Electrical power decreases by 10.42 W for each 10% shading conditions.

4.7. Electrical Efficiency. Figures 14(a)–14(d) show the percentage of η_e of the PVT system as a function of G, mass flow rate, T_{amb}, and partial shading, ranging from 200 to 500 W/m^2, 30 to 180 L/h, 10 to 37 °C, and 0 to 30%. The η_e of the system decreases as G increases, as shown in Figure 13(a). At the highest flow rate of 180 L/h, the electrical efficiency of the system drops from 14.5 to 14% as the irradiance level rises. As a result, for each 100 W/m^2 increase in G, electrical efficiency (η_e) decreases by about 0.167%.

Figure 14(b) represents that the maximum electrical efficiency is around 14%. For the cooling system, an inlet fluid flow rate of 180 L/h is preferable. For every 10 L/h
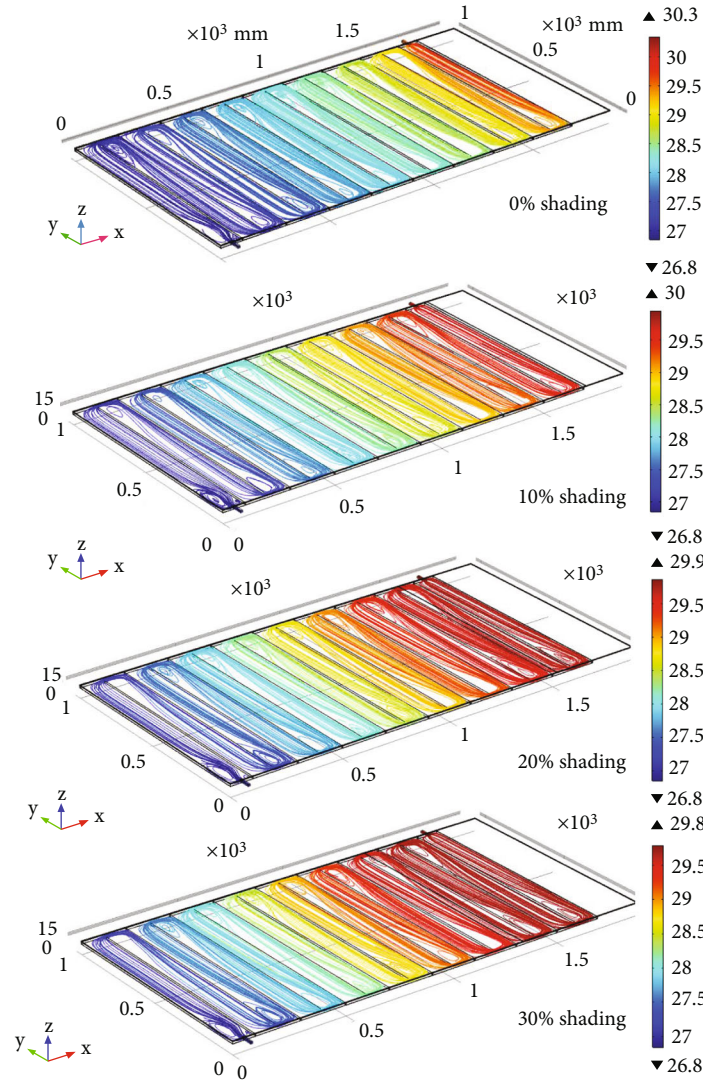
FIGURE 11: Outcome of partial shading on PVT streamlines plot with $G = 500$ W/m^2, $V_{in} = 180$ L/h, and $T_{amb} = 27°$C.

development in fluid flow rate, electrical efficiency increases by about 0.04%. The average temperature of the cell is reduced as the incoming mass flow rate of water increases. As a result, PVT current decreases marginally while PVT voltage rises noticeably which rises the output power and η_e.

The electrical efficiency (η_e) with the variation of T_{amb} is displayed in Figure 14(c). From the figure, for ambient temperatures of 10, 17, 27, and 37 °C, respectively, the electrical efficiency of PVT systems decreases by 14.2, 14.1, 14, and 13.9%. In this research, it is seen that, for each 1 °C increase in T_{amb}, electrical efficiency reduced about 0.01%.

The efficiency of solar modules is inversely proportional to shade. Figure 14(d) shows that the electrical efficiency is 14% with 500 W/m^2 irradiance and no shade. The electrical efficiency dropped to 12.7% after reaching 10% shading. When 20% of the PVT surface is shaded, the efficiency drops to 11.3%. Finally, the electrical efficiency decreased to 10% when 30% of the PVT top surface was shaded. The efficiency at 0% shading is more than that of 10–30% shading. As a

result, the shading patterns have a substantial impact on the module's PVT performance.

4.8. Outlet Fluid Temperature. The change of output fluid temperature for the effect of G (200-500 W/m^2), flow rate (30-180 L/h), T_{amb} (10-37°C), and partial shading (0-30%) is depicted in Figures 15(a)–15(d). As irradiance levels rise, the temperature of the fluid output rises. When the intensity of G is 200 W/m^2, the T_{out} is approximately 28.12 °C at a fixed mass flow rate of 180 L/h and T_{in} of 27 °C as shown in Figure 15(a). The fluid outlet means temperature increases to 28.67 °C at 300 W/m^2, 29.20 °C at 400 W/m^2, and 29.74 °C at the highest G of 500 W/m^2. Moreover, T_{out} increases by approximately 0.54 °C for each increment of 100 W/m^2 of G.

Figure 15(b) shows that, at a given T_{in} of 27 °C and G of 500 W/m^2, the T_{out} drops as the inlet flow rate rises. The increased convection heat transfer rate with increasing velocity might also be responsible for the downward trend. As the flow velocity rises, the rate of heat removal rises as
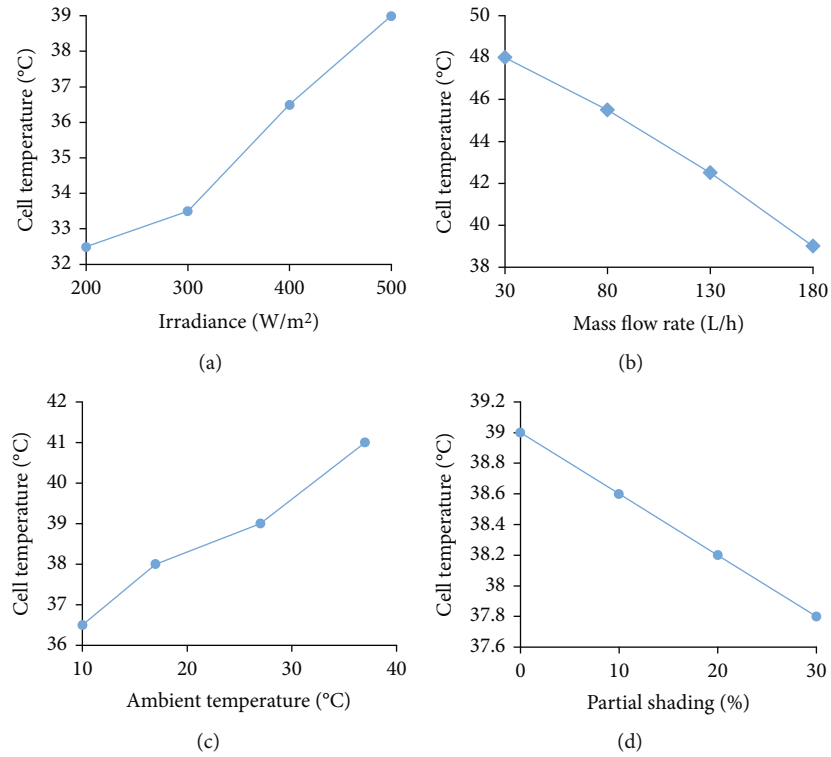
FIGURE 12: Outcome of (a) G, (b) V_{in}, (c) T_{amb}, and (d) partial shading on the temperature of solar cell.
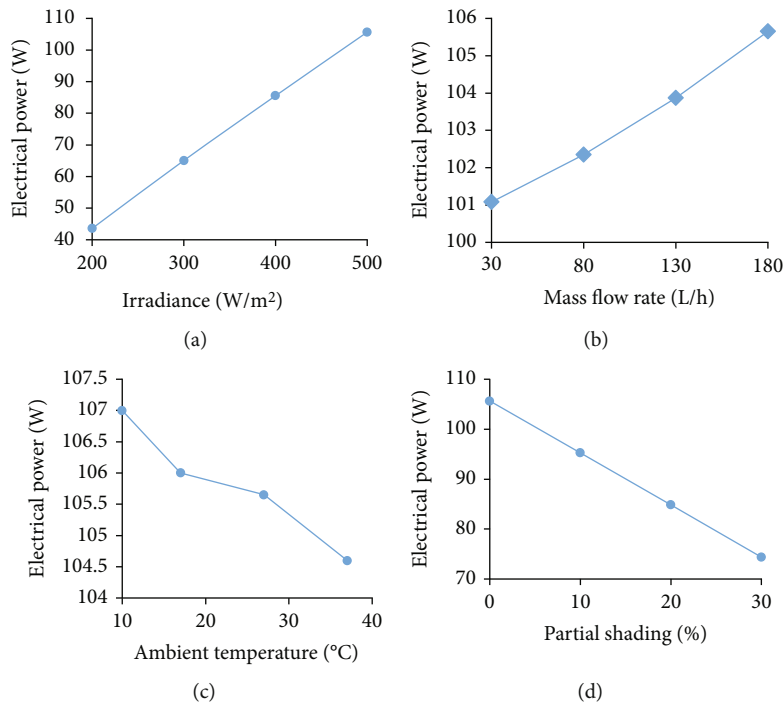

FIGURE 13: Outcome of (a) G, (b) V_{in}, (c) T_{amb}, and (d) partial shading on PVT electrical power.

well, leaving less time for thermal accumulation, lowering the T_{out}. When the flow rate is 30 L/h, the T_{out} is approximately 42.1 °C, and at the highest flow rate 180 L/h, the output fluid temperature is around 29.74 °C. Moreover, outlet fluid temperature decreases by approximately 0.83 °C for

each increment of 10 L/h flow rate. Up to a 180 L/h cooling water flow rate, this declining trend changes dramatically. As the flow rate rises, it lowers somewhat until it reaches 180 L/h. As a result, the flow rate of 180 L/h is the best for increasing the PVT system's efficiency.
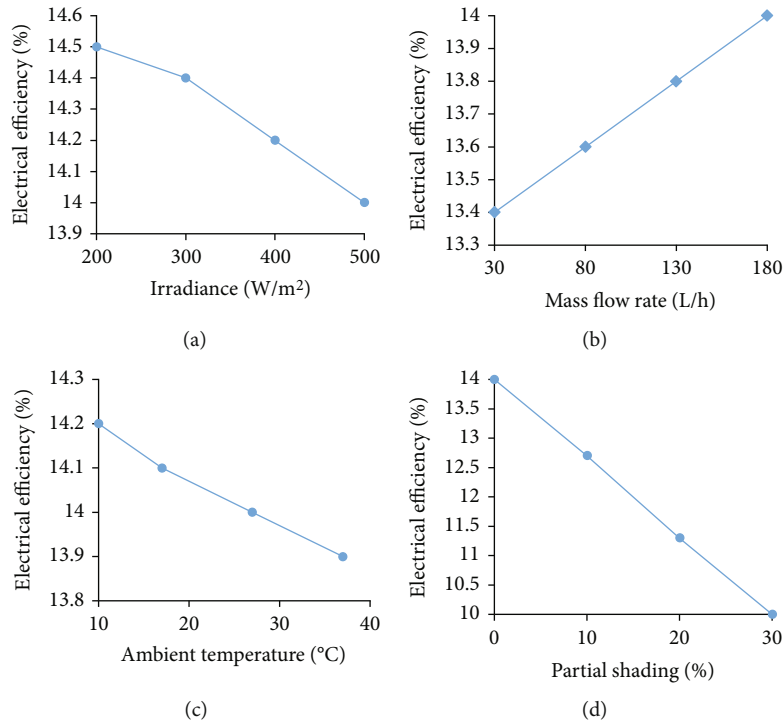
(a)

(b)

(c)

(d)

FIGURE 14: Outcome of (a) G, (b) V_{in}, (c) T_{amb}, and (d) partial shading on PVT electrical efficiency.
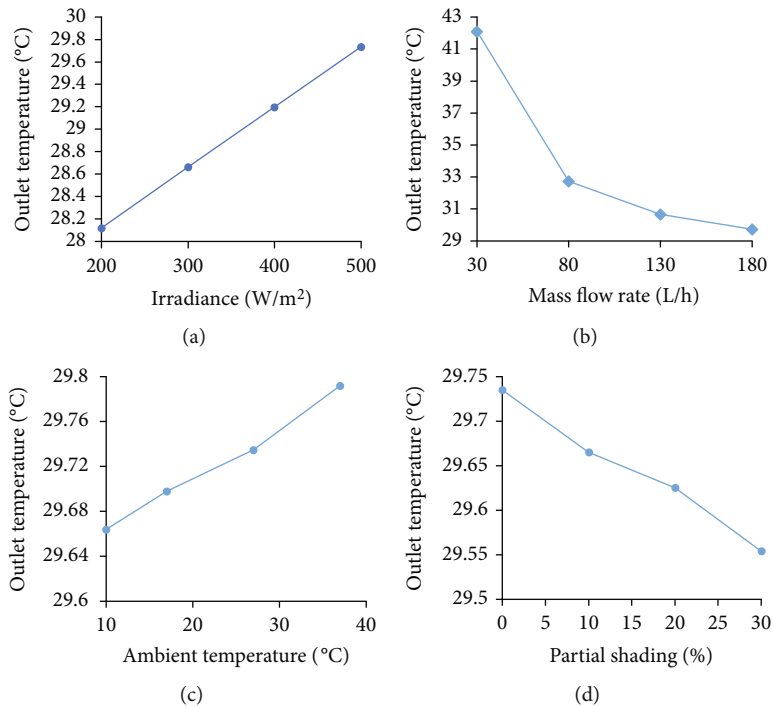

(a)

(b)

(c)

(d)

FIGURE 15: Outcome of (a) G, (b) V_{in}, (c) T_{amb}, and (d) partial shading on PVT output water temperature.

The T_{out} with the variation of T_{amb} at a fixed level of G of 500 W/m² is displayed in Figure 15(c). From the figure, for ambient temperatures of 10, 17, 27, and 37 °C, respectively, the outlet temperature of the PVT system is 29.66 °C, 29.7 °C, 29.74 °C, and 29.79 °C. For each 10 °C increase in inlet temperature, outlet temperature increased about 0.05 °C.

Shade has an inverse relationship with solar module outlet temperature. With 500 W/m² irradiance and no shade, the outlet temperature is 29.74 °C in Figure 15(d). After achieving 10% shading, the outlet temperature dropped to 29.67 °C. The outlet temperature drops to 29.63 °C when 20% of the PVT surface is shaded. When 30% of the top
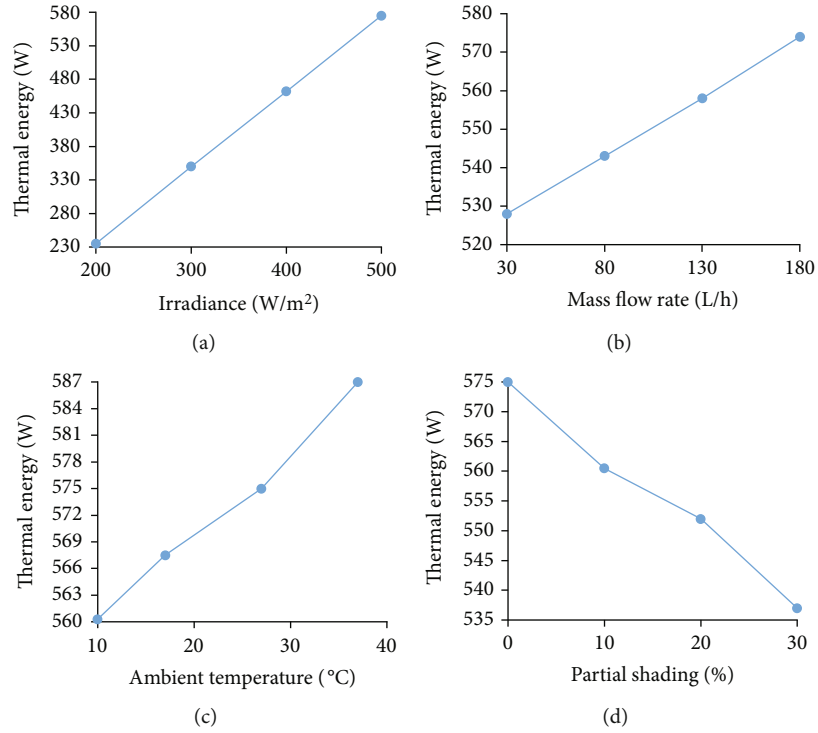
(a)

(b)

(c)

(d)

FIGURE 16: Outcome of (a) G, (b) V_{in}, (c) T_{amb}, and (d) partial shading on PVT thermal energy.
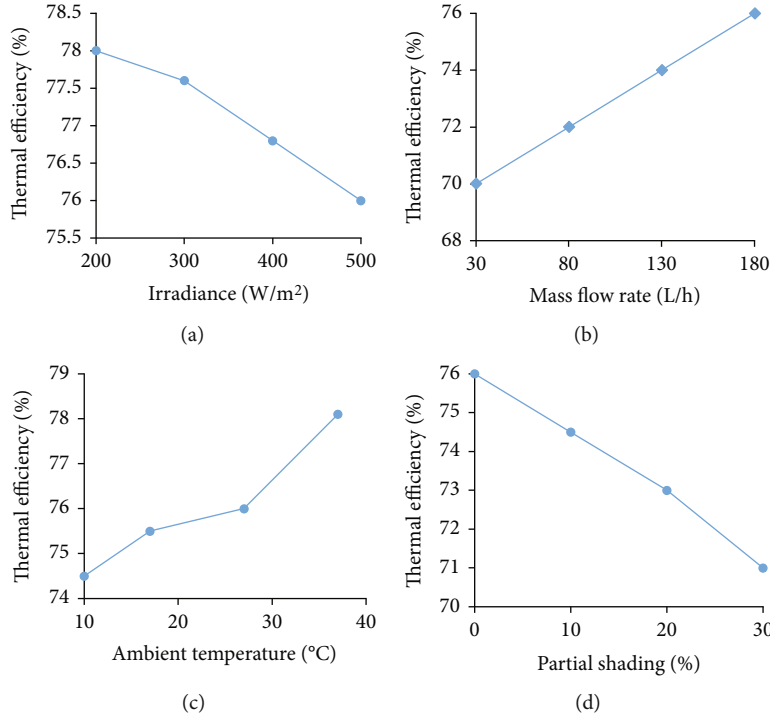

(a)

(b)

(c)

(d)

FIGURE 17: Outcome of (a) G, (b) V_{in}, (c) T_{amb}, and (d) partial shading on PVT thermal efficiency.

surface of the PVT was shaded, the outlet temperature decreased to around 29.55 °C. At 0% shading, the PVT system's outlet temperature is significantly higher than at 10–30% shading. For each 10% shading condition of the PVT system, outlet temperature decrease to 0.06 °C.

4.9. Thermal Energy. Figures 16(a)–16(d) depict the extracted E_t from the system as a function of G, flow rate, T_{amb}, and partial shading. The extracted E_t in the PVT system at 200 W/m^2 irradiance is 235 W. For the level of 500 W/m^2 of G and a fixed mass flow rate of 180 L/h, this energy
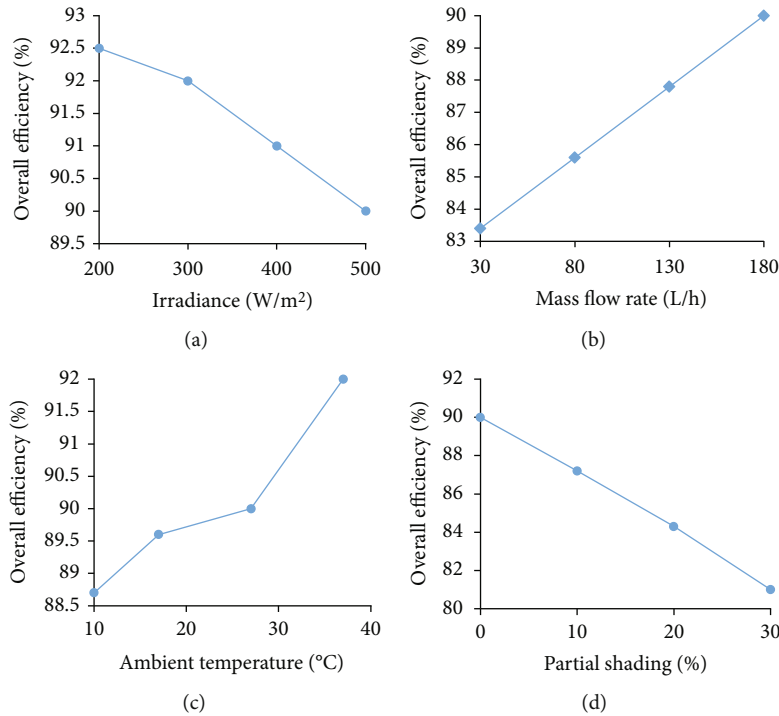
FIGURE 18: Outcome of (a) G, (b) V_{in}, (c) T_{amb}, and (d) partial shading on PVT overall efficiency.

TABLE 4: Comparison of PVT cell temperature among different studies.

Research	G (W/m^2)		Functioning temperature (°C)		Maximum T_{amb} (°C)	T_{sc} (°C) increment per G =100 W/m^2
	At initial period	At ultimate period	At initial period	At ultimate period		
Rahman et al. [3]	312	995	31	50	35	2.71
Chandrasekar et al. [24]	600	1300	40	50	37	1.4
Bahaidarah et al. [26]	240	979	21	35	21	1.9
Teo et al. [28]	550	1050	41	48		1.4
Current investigation	200	500	27	40.4	27	2.17

becomes 575 W. This is due to convective heat flow from the heat exchanger to the moving fluid as well conductive heat flow from the glass surface of the heat exchanger. Therefore, the difference between the T_{out} and T_{in} of fluids increases, allowing for more irradiance. Figure 16(a) indicates that for every 100 W/m^2 increase in G, the system extracts 113.3 W thermal energy.

When the flow rate is 30 L/h, the total quantity of E_t gathered from the system is 528 W. The amount of E_t is found to be 574 W at the greatest flow rate of 180 L/h as shown in Figure 16(b). However, increasing the cooling fluid flow rate (from 30 to 180 L/h) has a considerable impact on the rate at which the temperature of the outlet fluid drops. When the flow rate is increased to 180 L/h, the temperature of the exit fluid gradually declines. As a result, when the cooling fluid flow rate exceeds 180 L/h, the extracted thermal energy from the system gradually improves. The extracted thermal energy is 3.07 W for every 10 L/h increase in mass flow rate.

The E_t with the variation of T_{amb} at a fixed level of 500 W/m^2 of G is displayed in Figure 16(c). From the figure, for the T_{amb} of 10, 17, 27, and 37 °C, respectively, the E_t of PVT system is 560.3 W, 567.5 W, 575 W, and 587 W. It is clear to observe that, for each 10 °C increase in inlet temperature, thermal energy increased about 9.89 W.

The thermal energy of a solar module has an inverse relationship with shade. When the irradiance is 500 W/m^2 and there is no shadow, the thermal energy is 575 W, as shown in Figure 16(d). The thermal energy was reduced to 560.5 W after attaining 10% shading. When 20% of the PVT surface is shadowed, the thermal energy lowers to 552 W. The thermal energy dropped to roughly 537 W when 30% of the top surface of the PVT was shaded. For each 10% increase in partial shading, thermal energy decreased about 12.67 W.

4.10. Thermal Efficiency. As a function of G, flow rate, T_{amb}, and partial shading, Figures 17(a)–17(d) displays the η_t of

the system. It may be detected in Figure 17(a) that, when the level of G increases from 200 to 500 W/m^2, the η_t decreases at a given flow rate of 180 L/h. With a change in irradiance, η_t drops from 78% to 76%. For every 100 W/m^2 increase in solar irradiance, there is a 0.67% decrease in thermal efficiency.

The convective heat transfer coefficient of water is improved by increasing the flow rate from 30 to 180 L/h. As a result, more heat is transmitted at greater velocities under a given temperature difference, enhancing thermal efficiency. Here, the η_t rises from 70% to 76% in terms of flow rate. The fluid flow rate varies from 30 to 180 L/h, which makes increasing the efficiency rate difficult. Moreover, for a flow rate of 210 L/h, there is only a minor increase in η_t. The fact is that as the mass flow rate of cooling fluid increases (up to 180 L/h), the temperature of solar cells gradually drops. From Figure 17(b), when the mass flow rate of inlet water is increased by 10 L/h, the η_t increases by about 0.4%.

Figure 17(c) shows the thermal efficiency as a function of T_{amb} at a fixed level of 500 W/m^2 of G. The η_t of PVT systems is 74.5, 75.5, 76, and 78.1%, respectively, for ambient temperatures of 10, 17, 27, and 37 °C. It is easy to see how a 10 °C rise in inlet temperature enhanced thermal efficiency by around 1.33%.

Figure 17(d) illustrates that under 500 W/m^2 of G and no shade conditions, the η_t is 76%. After achieving 10% shade, the thermal efficiency dropped to 74.5%. The thermal efficiency reduces to 73% when 20% of the PVT surface is shadowed. Finally, the thermal efficiency decreases to 71% when 30% of the PVT top surface is shaded. For each 10% increase in partial shading, thermal efficiency decreased by about 1.67%.

4.11. Overall Efficiency.

4.11. Overall Efficiency. The total efficiency graph of the PVT system for the effects of G, flow rate, T_{amb}, and partial shading is shown in Figures 18(a)–18(d). With increasing values of G from 200 to 500 W/m^2 at 180 L/h mass flow rate and 27 °C of T_{in}, it reduces from 92.5% to 90%. From Figure 17(a) each 100 W/m^2 increase in the level of G reduces overall efficiency by 0.83%.

Figure 18(b) indicates that the total efficiency rises as the η_e and η_t rise with the inlet fluid flow rate. As a result, at a lower flow rate of 30 L/h, the overall efficiency is 83.4%. When the flow rate is increased to 180 L/h, it increases dramatically by up to 90%. For every 10 L/h increase in mass flow rate, overall efficiency increases by 0.44%.

Figure 18(c) shows the total efficiency as a function of T_{amb} at a given irradiance level of 500 W/m^2. The overall efficiency of the system is 88.7, 89.6, 90, and 92%, respectively, for ambient temperatures of 10, 17, 27, and 37 °C. It is easy to see how a 10 °C increase in inlet temperature improves overall efficiency by around 1.2%. To increase the overall efficiency of a PVT system, the temperature of the inlet fluid is significant.

Partial shading is inversely proportional to the total efficiency of a PVT system, as shown in Figure 18(d). The overall efficiency is 90% with 500 W/m^2 irradiance and no shade.

The total efficiency declined to 87.2% after reaching 10% shading. When 20% of the PVT surface is shaded, the overall efficiency drops to 84.3%. Finally, the overall efficiency dropped to around 81% when 30% of the top surface of the PVT is shaded. The overall efficiency of the PVT module is significantly higher at 0% shade than at 10–30% shading. Moreover, for every 10% rise in partial shading, the overall efficiency decreases by 3%.

4.12. Comparison. The present numerical result has been compared with previously published studies like Rahman et al. [3], Chandrasekar et al. [24], and Bahaidarah et al. [26]. Chandrasekar et al. [24] found a reduced temperature of cell by 20 °C and increased output power by 6.5 W and electrical efficiency by 1.4% under outdoor operating conditions. Bahaidarah et al. [26] found a decreased temperature of cell by 20% and increased electrical efficiency approximately 9% via a back surface water-cooling system. Table 4 shows the abovementioned comparison. A good similar pattern is observed for the present numerical result with other experimental results.

5. Conclusion

The results demonstrate that solar irradiance, cooling fluid mass flow rate, T_{amb}, and partial shading have extensive outcomes on PVT acts. Various levels of irradiance, mass flow rates, ambient temperature, and partial shading have been used to achieve high PVT performance while maintaining an optimal cooling system under operating conditions in Bangladesh. Major conclusions can be enlisted as

(i) The optimal V_{in} is obtained about 180 L/h up to $G = 500$ W/m^2

(ii) Escalating each $G = 100$ W/m^2 rises the values of T_{sc}, T_{out}, E_p, and E_t about 2.17 and 0.54 °C, 20.7, and 113.3 W, respectively

(iii) The values of η_e, η_t, and η_o reduce about 0.17, 0.67, and 0.83% due to enhancing every $G = 100$ W/m^2

(iv) The values of T_{sc} and T_{out} decrease by 0.6, and 0.83 °C, respectively; E_p and E_t enhance by 0.30, and 3.07 W, respectively, for rising each $V_{in} = 10$ L/h

(v) The increment of each $V_{in} = 10$ L/h upsurge the values of η_e, η_t, and η_o approximately 0.04, 0.4, and 0.44%, respectively

(vi) For every 10 °C increments of ambient temperature, the values of T_{sc}, and T_{out} increase by 1.7 and 0.05 °C, respectively; E_p devalues to 0.9 W, and E_t enhances to 9.89 W

(vii) The values of T_{sc}, T_{out}, E_p, and E_t decrease by 0.4 °C, 0.06 °C, 10.42 W, and 12.67 W, respectively, for each 10% partial shading

(viii) For the increment of every 10% partial shading, the values of η_e, η_t, and η_o diminish by 1.33, 1.67, and 3%

Nomenclature

A: PVT surface area [m^2]
C_p: specific heat [J/kg^{1}K^1]
E_p: Power of electrical [W]
E_r: Energy receiving by PV [W]
E_t: Energy of thermal [W]
m: Thermal energy [W]
V: Velocity of water [m/s]
G: Solar irradiance [W/m^2]
P: Packing factor [%]
k: Thermal conductivity [W/m^{1}K^1]
T: Temperature [°C]
p: Pressure [kgm/s^2]
U: Coefficient of thermal transfer [W/m^{2}K^1]
u, v, w: Components of velocity along coordinates direction [m/s^1]
x, y, z: Coordinates of Cartesian [m].

Abbreviations

FEM: Finite element method
HTF: Heat transferring fluid
PV: Photovoltaic
PVT: Photovoltaic thermal
2D: Two dimensional
3D: Three dimensional
PCM: Phase change material
PV: Photovoltaic
PVT: Photovoltaic thermal.

Greek Symbols

α: Absorptivity
β: Transmissivity
ε: Emissivity
ρ: Density [kg/m^3]
μ: Temperature coefficient
v: kinematic viscosity of the fluid [m^2/s^1]
η: Efficiency [%]
σ: Stefan-Boltzmann constant [W/m^{2}k^4].

Subscript

amb: Ambient
e: Electrical
t: Thermal
g: Glass
ga: Glass to ambient
gtd: Glass to tedlar
hea: Heat exchanger to ambient
he: Heat exchanger to water
r: Received
ref: Reference
sc: Solar cell
td: Tedlar
f: Fluid
in: Input
out: Output.

Data Availability

No data were used to support this study.

Conflicts of Interest

The authors declare that they have no conflicts of interest.

Acknowledgments

References

[1] R. Nasrin and M. Hossain, "Numerical analysis of photovoltaic power generation in different locations of Bangladesh," *Journal of Computational & Applied Research in Mechanical Engineering*, vol. 10, no. 2, pp. 373–389, 2021.

[2] M. M. Rahman, M. Hasanuzzaman, and N. A. Rahim, "Effects of various parameters on PV-module power and efficiency," *Energy Conversion and Management*, vol. 103, pp. 348–358, 2015.

[3] M. M. Rahman, M. Hasanuzzaman, and N. A. Rahim, "Effects of operational conditions on the energy efficiency of photovoltaic modules operating in Malaysia," *Journal of Cleaner Production*, vol. 143, pp. 912–924, 2017.

[4] A. A. El-Sebaii, F. S. Al-Hazmi, A. A. Al-Ghamdi, and S. J. Yaghmour, "Global, direct and diffuse solar radiation on horizontal and tilted surfaces in Jeddah, Saudi Arabia," *Saudi Arabia. Applied Energy*, vol. 87, no. 2, pp. 568–576, 2010.

[5] H. Hussein, G. Ahmad, and H. El-Ghetany, "Performance evaluation of photovoltaic modules at different tilt angles and orientations," *Energy Conversion and Management*, vol. 45, no. 15-16, pp. 2441–2452, 2004.

[6] P. Singh and N. M. Ravindra, "Temperature dependence of solar cell performance an analysis," *Solar Energy Materials and Solar Cells*, vol. 101, pp. 36–45, 2012.

[7] R. Nasrin, M. Hasanuzzaman, and N. A. Rahim, "Effect of high irradiation on photovoltaic power and energy," *International Journal of Energy Research*, vol. 42, no. 3, pp. 1115–1131, 2018.

[8] R. Nasrin, M. Hasanuzzaman, and N. A. Rahim, "Effect of high irradiation and cooling on power, energy and performance of a PVT system," *Renewable Energy*, vol. 116, pp. 552–569, 2018.

[9] A. Nahar, M. Hasanuzzaman, and N. A. Rahim, "Numerical and experimental investigation on the performance of a photovoltaic thermal collector with parallel plate flow channel under different operating conditions in Malaysia," *Solar Energy*, vol. 144, pp. 517–528, 2017.

[10] H. Fayaz, N. A. Rahim, M. Hasanuzzaman, R. Nasrin, and A. Rivai, "Numerical and experimental investigation of the effect of operating conditions on performance of PVT and PVT-PCM," *Renewable Energy*, vol. 143, pp. 827–841, 2019.

[11] M. Ashikuzzaman, R. Nasrin, F. T. Zohora, and M. S. Hossain, "3D study of heat transfer based on PVT/PCM system," in *AIP conference proceedings*, vol. 2121no. 1, AIP Publishing LLC, p. 120007, 2019.

[12] H. Fayaz, N. A. Rahim, M. Hasanuzzaman, A. Rivai, and R. Nasrin, "Numerical and outdoor real time experimental investigation of performance of PCM based PVT system," *Solar Energy*, vol. 179, pp. 135–150, 2019.

[13] R. Nasrin, M. Hasanuzzaman, and N. A. Rahim, "Effect of nanofluids on heat transfer and cooling system of the photovoltaic/thermal performance," *International Journal of Numerical Methods for Heat and Fluid Flow*, vol. 29, pp. 0961–5539, 2019.

[14] R. Nasrin, N. A. Rahim, H. Fayaz, and M. Hasanuzzaman, "Water/MWCNT nanofluid based cooling system of PVT: experimental and numerical research," *Renewable Energy*, vol. 121, pp. 286–300, 2018.

[15] S. Odeh and M. Behnia, "Improving photovoltaic module efficiency using water cooling," *Heat Transfer Engineering*, vol. 30, no. 6, pp. 499–505, 2009.

[16] M. A. Al Mamun, M. Hasanuzzaman, and J. Selveraj, "Experimental investigation of the effect of partial shading on photovoltaic performance," *IET Renewable Power Generation*, vol. 11, no. 7, pp. 912–921, 2017.

[17] A. J. Hanson, C. A. Deline, S. M. Mac Alpine, J. T. Stauth, and C. R. Sullivan, "Partial-shading assessment of photovoltaic installations via module-level monitoring," *IEEE Journal of Photovoltaics*, vol. 4, no. 6, pp. 1618–1624, 2014.

[18] J. Ahmed and Z. Salam, "A critical evaluation on maximum power point tracking methods for partial shading in PV systems," *Renewable and Sustainable Energy Reviews*, vol. 47, pp. 933–953, 2015.

[19] F. Belhachat and C. Larbes, "Modeling, analysis and comparison of solar photovoltaic array configurations under partial shading conditions," *Solar Energy*, vol. 120, pp. 399–418, 2015.

[20] A. Bidram, A. Davoudi, and R. S. Balog, "Control and circuit techniques to mitigate partial shading effects in photovoltaic arrays," *IEEE Journal of Photovoltaic*, vol. 2, no. 4, pp. 532–546, 2012.

[21] A. Dolara, G. C. Lazaroiu, S. Leva, and G. Manzolini, "Experimental investigation of partial shading scenarios on PV (photovoltaic) modules," *Energy*, vol. 55, pp. 466–475, 2013.

[22] R. Eke and C. Demircan, "Shading effect on the energy rating of two identical PV systems on a building façade," *Solar Energy*, vol. 122, pp. 48–57, 2015.

[23] A. Shukla, K. Kanta, A. Sharmaa, and P. H. Biwole, "Cooling methodologies of photovoltaic module for enhancing electrical efficiency: a review," *Solar Energy Materials and Solar Cells*, vol. 160, pp. 275–286, 2017.

[24] M. Chandrasekar, S. Suresh, T. Senthilkumar, and M. G. Karthikeyan, "Passive cooling of standalone flat PV module with cotton wick structures," *Energy Conversion and Management*, vol. 71, pp. 43–50, 2013.

[25] M. Hasanuzzaman, A. B. M. A. Malek, M. M. Islam, A. K. Pandey, and N. A. Rahim, "Global advancement of cooling technologies for PV systems: a review," *Solar Energy*, vol. 137, pp. 25–45, 2016.

[26] H. Bahaidarah, A. Subhan, P. Gandhidasan, and S. Rehman, "Performance evaluation of a PV (photovoltaic) module by back surface water cooling for hot climatic conditions," *Energy*, vol. 59, pp. 445–453, 2013.

[27] J. Jie, L. Jian-Ping, C. Tin-Tai, H. Wei, and P. Gang, "A sensitivity study of a hybrid photovoltaic/thermal water-heating system with natural circulation," *Applied Energy*, vol. 84, no. 2, pp. 222–237, 2007.

[28] H. G. Teo, P. S. Lee, and M. N. A. Hawlader, "An active cooling system for photovoltaic modules," *Applied Energy*, vol. 90, no. 1, pp. 309–315, 2012.

[29] K. S. Parlak, "PV array reconfiguration method under partial shading conditions," *International Journal of Electrical Power and Energy Systems*, vol. 63, pp. 713–721, 2014.

[30] K. Ishaque, Z. Salam, H. Taheri, and Syafaruddin, "Modeling and simulation of photovoltaic (PV) system during partial shading based on a two-diode model," *Simulation Modelling Practice and Theory*, vol. 19, no. 7, pp. 1613–1626, 2011.

[31] S. Kivrak, M. Gunduzalp, and F. Dincer, "Theoretical and experimental performance investigation of a two-axis solar tracker under the climatic condition of Denizli, Turkey," *Przegląd Elektrotechniczny*, vol. 88, no. 2, pp. 332–336, 2012.

[32] F. J. Gómez-Gil, X. Wang, and A. Barnett, "Energy production of photovoltaic systems: fixed, tracking, and concentrating," *Renewable and Sustainable Energy Reviews*, vol. 16, no. 1, pp. 306–313, 2012.

[33] S. Rustemli, F. Dincadam, and M. Demirtas, "Performance comparison of the sun tracking system and fixed system in the application of heating and lighting," *Arabian Journal for Science and Engineering*, vol. 35, 2010.

[34] H. Mousazadeh, A. Keyhani, A. Javadi, H. Mobli, K. Abrinia, and A. Sharifi, "A review of principle and sun-tracking methods for maximizing solar systems output," *Renewable and Sustainable Energy Reviews*, vol. 13, no. 8, pp. 1800–1818, 2009.

[35] R. Mamlook, S. Nijmeh, and S. M. Abdallah, "A programmable logic controller to control two axis sun tracking system," *Information Technology Journal*, vol. 5, no. 6, pp. 1083–1087, 2006.

[36] A. Kasaeian, Y. Khanjari, S. Golzari, O. Mahian, and S. Wongwises, "Effects of forced convection on the performance of a photovoltaic thermal system: an experimental study," *Experimental Thermal and Fluid Science*, vol. 85, pp. 13–21, 2017.

[37] M. Hosenuzzaman, N. A. Rahim, J. Selvaraj, A. B. M. A. Malek, and A. Nahar, "Global prospects, progress, policies, and environmental impact of solar photovoltaic power generation," *Renewable and Sustainable Energy Reviews*, vol. 41, pp. 284–297, 2015.

[38] U. Jahn and W. Nasse, "Operational performance of grid-connected PV systems on buildings in Germany," *Progress in Photovoltaics: Research and Applications*, vol. 12, no. 6, pp. 441–448, 2004.

[39] N. A. Kelly and T. L. Gibson, "Improved photovoltaic energy output for cloudy conditions with a solar tracking system," *Solar Energy*, vol. 83, no. 11, pp. 2092–2102, 2009.

[40] S. M. MacAlpine, R. W. Erickson, and M. J. Brandemuehl, "Characterization of power optimizer potential to increase energy capture in photovoltaic systems operating under nonuniform conditions," *IEEE Transactions on Power Electronics*, vol. 28, no. 6, pp. 2936–2945, 2013.

[41] S. Rasachak, U. Ghafoor, L. Kumar et al., "Effect of Tin Oxide/Black Paint Coating on Absorber Plate Temperature for Improved Solar Still Production: A Controlled Indoor and Outdoor Investigation," *International Journal of Photoenergy*, vol. 2022, Article ID 6902783, 12 pages, 2022.

[42] O. C. Zienkiewicz and R. L. Taylor, *The Finite Element Method*, McGraw-Hill, Fourth edition, 1991.

[43] R. Nasrin, "A 3D Numerical Study of Thermo-Fluid Characteristics of a Flat Plate Solar Collector Using Nanofluid," *Ph. D. Thesis*, Department of Mathematics, Bangladesh University of Engineering and Technology, Dhaka, Bangladesh, 2015.